Infrared Spectrum of Hydrogenated Corannulene *rim*-$HC_{20}H_{10}$ Isolated in Solid *para*-Hydrogen

Pavithraa Sundararajan,[1] Masashi Tsuge,[1,2,a)] Masaaki Baba,[3] Hidehiro Sakurai,[4] and Yuan-Pern Lee[1,5,6,a)]

[1]Department of Applied Chemistry and Institute of Molecular Science, National Chiao Tung University, Hsinchu 30010, Taiwan.

[2]Institute of Low Temperature Science, Hokkaido University, Sapporo 060-0819, Japan.

[3]Division of Chemistry, Graduate School of Science, Kyoto University, Kyoto 606-8502, Japan.

[4]Department of Applied Chemistry, Graduate School of Engineering, Osaka University, Osaka 565-0871, Japan.

[5]Center for Emergent Functional Matter Science, National Chiao Tung University, Hsinchu 30010, Taiwan.

[6]Institute of Atomic and Molecular Sciences, Academia Sinica, Taipei 10617, Taiwan.

[a)]Authors to whom correspondence should be addressed.
Electronic addresses: tsuge@lowtem.hokudai.ac.jp and yplee@nctu.edu.tw.
Telephone: +886-3-5131459.

Keywords:

Corannulene, hydrogenation, astrochemistry, *p*-H_2 matrix, IR spectroscopy

Abstract

Hydrogenated polycyclic aromatic hydrocarbons have been proposed to be carriers of the interstellar unidentified infrared (UIR) emission bands and the catalysts for formation of H_2; spectral characterizations of these species are hence important. We report the infrared (IR) spectrum of mono-hydrogenated corannulene ($HC_{20}H_{10}$) in solid *para*-hydrogen (*p*-H_2). In experiments of electron bombardment of a mixture of corannulene and *p*-H_2 during deposition of a matrix at 3.2 K, two groups of spectral lines increased with time during maintenance of the matrix in darkness after deposition. Lines in one group were assigned to the most stable isomer of hydrogenated corannulene, *rim*-$HC_{20}H_{10}$, according to the expected chemistry and a comparison with scaled harmonic vibrational wavenumbers and IR intensities predicted with the B3PW91/6-311++G(2d,2p) method. The lines in the other group do not agree with predicted spectra of other $HC_{20}H_{10}$ isomers and remain unassigned. Alternative hydrogenation was achieved with H-atoms produced photochemically in the infrared-induced reaction Cl + H_2 (v = 1) → H + HCl in a Cl_2/$C_{20}H_{10}$/*p*-H_2 matrix. With this method, only lines attributable to *rim*-$HC_{20}H_{10}$ were observed, indicating that hydrogenation via a quantum-mechanical tunneling mechanism produces preferably the least-energy *rim*-$HC_{20}H_{10}$ regardless of similar barrier heights and widths for the formation of *rim*-$HC_{20}H_{10}$ and *hub*-$HC_{20}H_{10}$. The mechanisms of formation in both experiments are discussed. The bands near 3.3 and 3.4 μm of *rim*-$HC_{20}H_{10}$ agree with the UIR emission bands in position and relative intensity, but other bands do not match satisfactorily with the UIR bands.

I. INTRODUCTION

Polycyclic aromatic hydrocarbons (PAH) are ubiquitous in the interstellar media (ISM).[1] These molecules, composed primarily of carbon in fused rings, are believed to be the carbon compound of the most common class in the galaxy, meteorites, cometary, and cosmic dust. PAH and their derivatives are considered as possible candidates for the carriers of the interstellar unidentified infrared (UIR) emission bands.[2,3,4] The 3.4-μm feature observed in the UIR emission has been postulated to originate from aliphatic CH stretching vibration modes of hydrogenated PAH.[5] Spectral signatures of hydrogenated PAH identified in a laboratory will help to assess this hypothesis and, moreover, enable observers to probe these species in the ISM.

In addition, PAH and their derivatives have been suggested to be able to catalyze the formation of H_2.[6,7,8,9,10] Because H_2 is the most abundant molecule in the universe,[11,12,13] its formation and evolution in the interstellar space are important in many astrochemical processes. Gaseous reactions involving H-atom recombination, radiative association, and other processes to produce H_2 molecules are too slow to account for the abundance of H_2 in the ISM.[12] The main route for the formation of H_2 is hence generally assumed to occur through the recombination of H-atoms on dust grain surfaces.[9,14,15,16,17,18] A physisorbed hydrogen atom can combine with another hydrogen atom to form H_2, which eventually evaporates into space, but these processes require very low temperature, 10–20 K. H_2 formation via this mechanism cannot occur in the photodissociation regions where dust and gas temperatures are higher. However, high H_2 formation rates have been observed in the

photodissociation region. In order to explain the observed rates, we need to consider other mechanisms responsible for the H_2 formation,[19] and one proposed mechanism is the H_2 formation catalyzed by PAH and their derivatives. The proposed model for H_2 formation with PAH involves the capture of a hydrogen atom by a neutral PAH, H + PAH → HPAH, or by a PAH cation (designated PAH^+), $H + PAH^+ \rightarrow H^+PAH$, in which HPAH and H^+PAH denote mono-hydrogenated PAH and mono-protonated PAH, respectively. When a second H-atom extracts an excess hydrogen from HPAH or H^+PAH, molecular hydrogen can be formed.

We have recorded the infrared (IR) spectra of several HPAH and H^+PAH in solid *p*-H_2 that were produced by electron bombardment on PAH/*p*-H_2 mixtures during deposition at 3.2 K. The advantages of our method include negligible fragmentation, narrow spectral lines, true absorption intensity, and wide spectral coverage. This method has been applied to benzene (C_6H_6),[20] naphthalene ($C_{10}H_8$),[21] pyrene ($C_{16}H_{10}$),[22] coronene ($C_{24}H_{12}$),[23] and ovalene ($C_{32}H_{14}$)[24] to obtain IR spectra of their protonated and mono-hydrogenated species. That the reactions H + PAH → HPAH can occur via quantum tunneling of H-atom through small reaction barriers even at the low temperatures relevant to astronomical conditions has been demonstrated.[25,26]

Extending our research to corannulene ($C_{20}H_{10}$), a bowl-shaped PAH that is considered to be a fragment of C_{60},[27] we reported recently the IR spectra of protonated corannulene isomers (*hub*-$H^+C_{20}H_{10}$ and *rim*-$H^+C_{20}H_{10}$).[28] The IR spectrum of *hub*-$H^+C_{20}H_{10}$ matches well the UIR emission bands, consistent with the suggestions that H^+PAH and non-planar PAH (and their derivatives) might

be important contributors to the UIR bands.[4,29] Hydrogenated corannulene ($HC_{20}H_{10}$) might consequently be present also in the ISM. Experiments on protonated corannulene in the gaseous phase[30] and in solid *p*-H_2[28] are known, but, to our knowledge, no experiment on hydrogenated corannulene has been reported. The tentative assignments of a few IR lines of $HC_{20}H_{10}$ observed in our preliminary experiments were presented recently.[31] We report here the full IR assignments of the most stable isomer of hydrogenated corannulene (*rim*-$HC_{20}H_{10}$) in solid *p*-H_2.

II. METHODS

Our experimental setup for *p*-H_2 matrix isolation is described elsewhere.[20,32] In brief, the experiments were performed with a closed-cycle helium-refrigerator system capable of cooling a gold-coated copper substrate to 3.2 K; this copper plate serves also as a mirror to reflect the incident IR beam to the detector. A Fourier-transform infrared (FTIR) spectrometer, equipped with a KBr beam splitter and a Hg-Cd-Te detector (77 K), was used to record IR spectra in a spectral range 400–5000 cm^{-1}. Spectra were recorded with resolution 0.25 cm^{-1} and averaged over 500 scans at each stage of an experiment.[25]

Two methods were utilized to produce hydrogenated corannulene. In the first method, gaseous mixtures of $C_{20}H_{10}$/*p*-H_2 were bombarded with electrons during deposition of a matrix at 3.2 K. The electrons ionized H_2 to produce H_2^+ that readily reacted with another H_2 to form H_3^+ and H-atom;[33] reactions of H_3^+ and H with corannulene led to protonated and mono-hydrogenated corannulene,

respectively. In the second method, a $Cl_2/C_{20}H_{10}/p\text{-}H_2$ matrix was photolyzed to produce Cl atoms; subsequent irradiation of the matrix with IR light induced the reaction $Cl + H_2$ ($v = 1$) $\rightarrow$ H + HCl.[34,35] The H-atom thus produced was mobile and could react effectively with corannulene.

In the electron-bombardment experiment, gaseous mixtures of $C_{20}H_{10}/p\text{-}H_2$ were prepared *in situ* during deposition. *Para*-H_2 was passed through a stainless steel tube (outer diameter 6 mm) containing corannulene ($C_{20}H_{10}$, >94 % purity, Kanto Chemical); the tube was heated to 408 K to increase the vapor pressure of the sample.[28] The gaseous mixture of $C_{20}H_{10}/p\text{-}H_2$ was deposited onto the substrate at 3.2 K over a period of 10 h at a flow rate ~12 mmol h^{-1}. We estimated the mixing ratio of $C_{20}H_{10}/p\text{-}H_2$ in these experiments to be 3.0 ± 0.3 ppm according to the method of Ruzi *et al.*[36] using the estimated matrix thickness and quantum-chemically predicted IR intensities of some intense lines of corannulene; the error represents only the fitting error from various lines, whereas the actual relative error might be as great as 50 %. The matrix was bombarded with an electron beam during deposition with current 30 μA and kinetic energy 270 eV. To distinguish the hydrogenated species from various species produced after electron bombardment, we maintained the matrix in darkness for 30 h. Secondary photolysis was subsequently performed with light at 520, 445, and 365 nm from light-emitting diodes and at 254 nm from a low-pressure Hg lamp.

In the $Cl_2/C_{20}H_{10}/p\text{-}H_2$ experiments, a $C_{20}H_{10}/p\text{-}H_2$ mixture and a small amount of Cl_2 gas were co-deposited over a period of 8 h with flow rate ~12.5 mmol h^{-1} of $C_{20}H_{10}/p\text{-}H_2$; the temperature of the corannulene sample was set at 415 K. The flow rate of Cl_2 was adjusted to obtain a matrix with

an approximate mixing ratio $Cl_2/C_{20}H_{10}/p\text{-}H_2 \approx 50/1/100{,}000$. After deposition at 3.2 K, the matrix was irradiated with light at 405 nm from a diode laser (20 mW), followed by irradiation with IR light from a water-cooled Globar source. We employed light at 405 nm instead of the absorbance maximum of Cl_2 near 365 nm to avoid unwanted photolysis of corannulene.[28] During photolysis and acquisition of spectra, a long-pass filter (LP-2500 nm, Spectrogon) blocking light above 4000 cm^{-1} was employed to avoid the reaction between Cl and *p*-H_2. Several ratios of $Cl_2/C_{20}H_{10}$ and varied durations of visible and IR irradiations were investigated to achieve a better yield of hydrogenated products. To differentiate the products further, secondary photolysis was performed with light at 460 nm for 30 min and 365 nm for 30 min. *Para*-hydrogen was prepared in another closed-cycle helium-refrigerator system capable of cooling a 1/8″ copper tube, filled with $Fe(OH)_3$ catalyst, to 10 K. Normal-H_2 (99.9999 %) was typically passed through the tube with a conversion temperature set to 13 K.[32]

Quantum-chemical calculations were performed with Gaussian 09 (revisions C.01 and D.01). Geometrical optimization and harmonic vibrational analysis were performed with the B3PW91/6-311++G(2d,2p) method; this method has been applied to several PAH and H^+PAH investigated in our group; satisfactory agreements between predicted and observed IR spectra have been demonstrated.[31] To account for the difference in the extent of anharmonicity between the CH stretching and other vibrational modes, the harmonic vibrational wavenumbers were scaled with factors of 0.958 for values >2500 cm^{-1} and 0.978 for values <2500 cm^{-1}; these factors are the same

as those used for coronene,[23] ovalene,[26] and corannulene.[28] In calculations of relative energies, correction of zero-point vibrational energy (ZPVE) was performed with unscaled harmonic vibrational wavenumbers.

III. COMPUTATIONAL RESULTS

Corannulene has carbon atoms of three distinct types; one consists of carbon atoms of the inner five-membered ring, one consists of the unfused carbons of the outer benzenoid rings, and the other consists of the fused carbon of these outer rings, to which we refer as *hub*-, *rim*-, and *spoke*-carbons, respectively. The hydrogen atom can attack a carbon of each of these three types. We found four stable isomers of hydrogenated corannulene $HC_{20}H_{10}$; representative bond angles and bond lengths are presented in Fig. 1. The *spoke*-carbon can be hydrogenated from both convex and concave sides of the molecule; the former is designated *spoke*-$HC_{20}H_{10}$ and the latter *concave-spoke*-$HC_{20}H_{10}$. Hydrogenation at the *rim*-site leads to only one product, *rim*-$HC_{20}H_{10}$. Although, for the *hub*-carbon, hydrogen atom can attack it from both the convex and the concave sides, we found only one stable isomer, *hub*-$HC_{20}H_{10}$, with hydrogenation from the convex side. All attempts to optimize *concave-hub*-$HC_{20}H_{10}$ resulted in *concave-spoke*-$HC_{20}H_{10}$. The isomer of least energy is *rim*-$HC_{20}H_{10}$, whereas *hub*-$HC_{20}H_{10}$ and *spoke*-$HC_{20}H_{10}$ have energies greater by 17.2 and 64.4 kJ mol^{-1}, respectively; all energies are corrected for ZPVE. The energy of *concave-spoke*-$HC_{20}H_{10}$ is 127.3 kJ

mol^{-1} above that of *rim*-$HC_{20}H_{10}$, much greater than energies of the corresponding structures arising from hydrogenation at the convex side.

The potential-energy schemes for the hydrogenation of corannulene and the isomerization of hydrogenated corannulene are presented in Fig. 2. The energies of all four possible isomers of hydrogenated corannulene and the associated transition states (TS) for isomerization are listed in Table I. The formation of *hub*- or *spoke*-hydrogenated isomers from H + $C_{20}H_{10}$ has a barrier 10.7 or 22.4 kJ mol^{-1}, respectively. The barriers for the formation of the *rim*-isomer via attack from the convex and concave sides are 10.9 and 16.0 kJ mol^{-1}, respectively. The barrier for the formation of the *concave-spoke*-isomer is much greater, 45.8 kJ mol^{-1}. The barriers for the interconversion between isomers with neighboring hydrogenation sites are greater than the exothermicities of H + $C_{20}H_{10}$; once corannulene is hydrogenated in the tunneling reaction at low temperature, interconversion between them is hence unlikely.

Vibrational wavenumbers and IR intensities of the representative vibrational modes of *hub-, rim-*, and *spoke*-$HC_{20}H_{10}$, predicted with the B3PW91/6-311++G(2d,2p) method, are listed in Table II; the full lists of predicted values are available in Tables SI and SII. Those predicted for *concave-spoke*-$HC_{20}H_{10}$ are listed in Table SII. The isomers of $HC_{20}H_{10}$ have intense vibrational lines associated with the CH out-of-plane bending modes at 827.0 (ν_{54}) and 835.2 (ν_{53}) cm^{-1} for *rim*-$HC_{20}H_{10}$, 829.5 (ν_{53}) cm^{-1} for *hub*-$HC_{20}H_{10}$, and 823.3 (ν_{54}) and 847.2 (ν_{52}) cm^{-1} for *spoke*-$HC_{20}H_{10}$. The *rim*-$HC_{20}H_{10}$ has characteristic vibrational modes associated with the CH_2 moiety, with lines

associated with the CH_2 scissoring (mixed) mode predicted in region 1457.1–1407.2 (ν_{18}–ν_{24}) cm^{-1} and those with the CH_2 stretching modes predicted at 2828.3 (ν_{11}) and 2916.6 (ν_{10}) cm^{-1}. Vibrational lines of the CH stretching mode (ν_{11}) associated with the added H-atom are predicted at 2785.3 cm^{-1} for *hub*-$HC_{20}H_{10}$, 2717.0 cm^{-1} for *spoke*-$HC_{20}H_{10}$, and 2600.7 cm^{-1} for *concave-spoke*-$HC_{20}H_{10}$.

The UV-Vis absorption spectra of *rim*-, *hub*-, *spoke*-, and *concave-spoke*-$HC_{20}H_{10}$ predicted with the TD-B3PW91/6-311++G(2d,2p) method are shown in Fig. S1. The *rim*-, *hub*-, and *spoke*-$HC_{20}H_{10}$ isomers have similar absorption profiles with one weak line near 480–500 nm and an intense line near 300 nm. The absorption spectrum of *concave-spoke*-$HC_{20}H_{10}$ isomer has two features near 480 and 300 nm with similar intensities.

IV. EXPERIMENTAL RESULTS

A. Electron bombardment on $C_{20}H_{10}$/p-H_2 mixtures

Fig. 3(a) shows a partial IR spectrum of an electron-bombarded $C_{20}H_{10}$/*p*-H_2 matrix measured after deposition. The lines of $C_{20}H_{10}$ are stripped (i.e., the IR lines of the parent molecule are subtracted from the spectrum by using a spectrum of $C_{20}H_{10}$/*p*-H_2 matrix deposited without electron bombardment); lines present in this spectrum are hence all induced by electron bombardment. The spectra in the CH stretching region (3150–2750 cm^{-1}) are shown in Fig. S2. The electron bombardment of $C_{20}H_{10}$/*p*-H_2 mixtures during deposition produces both protonated and hydrogenated corannulene as discussed in our previous work.[28] To distinguish the protonated and hydrogenated

products, we maintained the matrix in darkness for 30 h during which the neutralization of the protonated corannulene, $HC_{20}H_{10}^{+} + e^{-} \rightarrow HC_{20}H_{10}$, and the H-atom addition to corannulene, $H + C_{20}H_{10} \rightarrow HC_{20}H_{10}$, occurred. As a consequence of these reactions, lines of $HC_{20}H_{10}$ are expected to increase in intensity with time. A difference spectrum obtained on subtracting the spectrum measured directly after deposition from one measured after 30 h is shown in Fig. 3(b).

During maintenance of the matrix in darkness for 30 h, lines marked A increased in intensity by ~20 % and those marked B increased by ~50 %. Group A consists of 26 lines with the most intense line at 827.1 cm^{-1} and lines with intensities ≥10 % of this most intense line, at 3051.2, 3048.1, 2908.2, 2792.3, 788.9, 768.3, 652.4, 638.6, 627.5, and 536.4 cm^{-1}, as listed in Table III. Group B consists of 15 lines with this most intense line at 822.7 cm^{-1}; these lines are also listed in Table III for comparison. Secondary photolysis was conducted at wavelengths 520, 445, 365, and 254 nm. At 365 and 445 nm, lines in groups A and B decreased to the same extent whereas no changes were observed upon irradiation at 520 and 254 nm. To be discussed in Sec. V-A, lines in group A are assigned to *rim*-$HC_{20}H_{10}$ and those in group B might be due to some fragments.

B. Photolysis of $Cl_2/C_{20}H_{10}/p$-H_2 matrices

After co-deposition of Cl_2 and $C_{20}H_{10}/p$-H_2, the matrix was subjected to photolysis at 405 nm for 1.5 h followed by IR irradiation for 3 h. The partial IR spectrum in the CH out-of-plane bending regions 860–750 and 680–600 cm^{-1}, with lines of $C_{20}H_{10}$ stripped, is shown in Fig. 4(a) and compared with the spectrum of an electron-bombarded $C_{20}H_{10}/p$-H_2 matrix shown in Fig. 4(b). The

comparison for region 1510–500 cm^{-1} is presented in Fig. S3. These comparisons indicate that, in a visible- and IR-irradiated $Cl_2/C_{20}H_{10}/p$-H_2 matrix, only one product (lines in group A) was produced. The wavenumbers and relative intensities of these lines are listed in Table III for comparison. This result allowed us to discriminate further lines in groups A and B.

V. DISCUSSION

A. Assignment of lines in group A to rim-$HC_{20}H_{10}$

As discussed in Sec IV-A, the increased intensity of lines in groups A and B during maintenance of the electron-bombarded matrix in darkness indicates that they might be associated with hydrogenated corannulene. Grouping of lines to A and B was achieved based on their behavior in darkness, the secondary photolysis, and the presence or absence in the $Cl_2/C_{20}H_{10}/p$-H_2 experiments. The IR spectrum of a $Cl_2/C_{20}H_{10}/p$-H_2 matrix measured after visible- and IR-irradiations is compared with quantum-chemically predicted IR spectra of *rim*-, *hub*-, and *spoke*-$HC_{20}H_{10}$ in Fig. 5; these predicted spectra were simulated according to the scaled harmonic vibrational wavenumbers and IR intensities calculated with the B3PW91/6-311++G(2d,2p) method. The spectrum of an electron-bombarded $C_{20}H_{10}/p$-H_2 matrix measured after deposition is also compared with these predicted spectra in Fig. S4.

According to the theoretical predictions (Table II), these three isomers of $HC_{20}H_{10}$ show distinct patterns in the spectral region 1500−500 cm^{-1}, with the most intense line in region 850−500 cm^{-1}. In

this region, for *rim*-$HC_{20}H_{10}$, six intense lines with IR intensities >10 km mol^{-1} are predicted near 835.2, **827.0**, 786.1, 651.0, 638.4, and 537.2 cm^{-1}; lines with intensities greater than 80 % of that of the most intense line are listed in bold face. For *hub*-$HC_{20}H_{10}$, six intense lines are predicted near **829.5**, 788.8, 775.4, 668.0, 642.3, and 529.0 cm^{-1} with IR intensities >10 km mol^{-1}. For *spoke*-$HC_{20}H_{10}$, seven intense lines are predicted near 979.6, **847.2**, **823.3**, 801.5, 660.6, 635.1, and 549.7 cm^{-1} with IR intensities >10 km mol^{-1}.

Five intense lines in group A with wavenumbers **827.1**, 788.9, 652.4, 638.6, and 536.4 cm^{-1}, with the most intense line in bold face, agree with those predicted for *rim*-$HC_{20}H_{10}$; the line predicted at 835.2 cm^{-1} was unobserved because of severe interference from the most intense line of $C_{20}H_{10}$ near 837 cm^{-1}. In addition to these lines, 8 lines in group A with moderate intensities at 1299.4, 1128.4, 1124.7, 947.5, 807.8, 768.3, 627.5, and 528.5 cm^{-1} were observed; their wavenumber and relative intensities agree satisfactorily with lines predicted at 1297.4, 1128.4, 1125.1, 947.5, 811.7, 763.8, 624.7, and 526.0 cm^{-1}, as compared in Table III. For the CH stretching modes above 3030 cm^{-1} (Fig. S5), because of spectral congestion, we provide only tentative assignments. The CH_2 stretching modes, which are characteristic of *rim*-$HC_{20}H_{10}$, were predicted at 2916.6 (ν_{10}) and 2828.3 (ν_{11}) cm^{-1} and observed at 2908.2 and 2792.3 cm^{-1}. The 26 lines in group A are hence assigned to *rim*-$HC_{20}H_{10}$ with mean absolute deviation 4.3 ± 1.4 cm^{-1}.

The spectrum of lines in group B observed in an electron-bombarded $C_{20}H_{10}$/*p*-H_2 matrix is compared in Fig. S4 with quantum-chemically predicted IR spectra of *rim*-, *hub*-, and *spoke*-

$HC_{20}H_{10}$. Below 1500 cm^{-1}, four intense lines in group B at **822.7**, 777.6, 761.7, and 656.4 cm^{-1} were observed. In addition to these lines, eleven lines were identified, as listed in Table III. These lines in group B do not agree with the predicted spectrum of *rim*- or *hub*- or *spoke*-$HC_{20}H_{10}$, indicating that the spectral carrier of lines in group B is not an isomer of $HC_{20}H_{10}$.

Depletion fractions upon secondary photolysis at 365 and 465 nm were similar for lines in groups A (*rim*-$HC_{20}H_{10}$) and B (unassigned product). According to the TD-DFT calculations with the B3PW91/6-311++G(2d,2p) method, *rim*-$HC_{20}H_{10}$ has absorption maxima near 300 and 480–500 nm (Fig. S1). The similarity between groups A and B upon secondary photolysis indicates that the spectral carrier of lines in group B might have a chromophore similar to that of *rim*-$HC_{20}H_{10}$.

We compared IR stick spectra of hydrogenated coronene (*rim*-$HC_{24}H_{12}$)[23] and hydrogenated corannulene (*rim*-$HC_{20}H_{10}$) in Fig. S6. The number of lines of *rim*-$HC_{24}H_{12}$ is smaller than that of *rim*-$HC_{20}H_{10}$ because of higher symmetry. The *rim*-$HC_{20}H_{10}$ has four intense lines in region 850–750 cm^{-1} corresponding to CH out-of-plane bending modes, but *rim*-$HC_{24}H_{12}$ possesses only two intense lines. In addition, for *rim*-$HC_{24}H_{12}$, the vibrations associated with ring deformation and combination modes in region below 700 cm^{-1} are unobserved due to small intensities except for the line observed at 541.0 cm^{-1} due to the combination of CH out-of-plane bending and CH_2 rocking modes.

B. Comparison with UIR emission bands

The UIR emission spectra typically exhibit bands near 3.3 μm (CH stretching modes, with a weak feature at 3.4 μm), 6.2 and 7.7 μm (CC stretching modes of aromatic ring), 8.6 μm (CH in-plane

bending modes), and 11.2 μm (CH out-of-plane bending modes). The hydrogenated PAH are of astronomical significance especially in studying the 3.3 and 3.4 μm bands of the UIR emission, which correspond to the aromatic and aliphatic CH stretching modes, respectively.[37] Several theoretical modelling and experimental studies have demonstrated that a PAH with an aliphatic side group could indeed contribute to the 3.4 μm band.[38] Fig. 6 presents a comparison of the IR spectra of *rim*-$HC_{20}H_{10}$ and the most stable protonated isomer *hub*-$H^+C_{20}H_{10}$ with the UIR bands from the Orion Bar PDR.[39] Because experimental spectra are IR absorption spectra of matrix-isolated species, they might differ slightly from the UIR bands originating from UV-induced emission.[24] For *rim*-$HC_{20}H_{10}$, the aromatic CH stretching mode is located at 3.28 μm and aliphatic CH stretching modes are located at 3.44 and 3.58 μm. The lines of the *rim*-$HC_{20}H_{10}$ at 3.28 and 3.44 μm are in close resemblance with the 3.3 and 3.4 μm bands of the UIR emission in terms of line positions and relative intensities.

The position of the CH stretching modes of the most stable protonated isomer, *hub*-$H^+C_{20}H_{10}$, is red-shifted to 3.62 μm, close to the weak 3.74-μm line of the UIR emission. Compared with the spectrum of *rim*-$HC_{20}H_{10}$, the laboratory spectrum of *hub*-$H^+C_{20}H_{10}$ is in close agreement with the UIR bands in the region 6–12 μm as discussed in our previous work.[28] When we compare the spectra of protonated and hydrogenated species, the enhancement of intensities of features in the protonated isomer (*hub*-$H^+C_{20}H_{10}$) near 6.2, 7.7, and 8.6 μm is evident, in general accordance with the argument that the 6.2, 7.7, and 8.6 μm bands are dominated by cationic/protonated PAH and the 3.3 and 11.2 μm are dominated by neutral PAH.[39] However, the lines of CH out-of-plane bending modes in

hydrogenated corannulene *rim*-$HC_{20}H_{10}$ extending from 11.8–13.5 μm agree poorly with the intense UIR band near 11.2 μm, but the corresponding line of the protonated species *hub*-$H^+C_{20}H_{10}$ agrees well with the UIR band.

C. Mechanism of formation

As discussed previously, in electron-bombardment experiments, $HC_{20}H_{10}$ was produced either via reaction of corannulene with an H-atom or on neutralization of protonated corannulene ($H^+C_{20}H_{10}$),[28] whereas, in the Vis/IR irradiation experiments of $Cl_2/C_{20}H_{10}/p$-H_2, $HC_{20}H_{10}$ was produced only via hydrogenation.

Because H-atom addition reactions to corannulene have small barriers (Fig. 2), these reactions can occur at low temperatures only through tunneling. According to calculations with the B3PW91/6-311++G(2d,2p) method, barrier heights for the formation of *rim*-, *hub*-, *spoke*-, and *concave-spoke*-$HC_{20}H_{10}$ are 10.9, 10.7, 22.4, and 45.8 kJ mol^{-1}, respectively; the barriers for *rim*- and *hub*-isomers are nearly identical, within computational accuracy. Calculations of the intrinsic reaction coordinate indicate that the widths of the barrier for the formation of *rim*- and *hub*-isomers are also practically the same, but, as discussed in Sec IV-B, the H-atom addition preferably favors the formation of *rim*-$HC_{20}H_{10}$ that has the least energy. Intuitively, the greater density of states for the formation of *rim*-$HC_{20}H_{10}$ might be the reason for this preference. In our previous experiments on H + ovalene ($C_{32}H_{14}$), we observed the formation of isomer 7-$C_{32}H_{15}$ of least energy that has a barrier ~10 kJ mol^{-1}; the next feasible channel producing 1-$C_{32}H_{15}$ has a barrier ~13 kJ mol^{-1} and

energy 31 kJ mol^{-1} above 7-$C_{32}H_{15}$, but was unobserved.[26]

In one experiment with the Vis/IR irradiation of $Cl_2/C_{20}H_{10}/p$-H_2, the mixing ratio of $C_{20}H_{10}$ decreased from 10.5 to 9.4 ppm (a decrease of 1.1 ppm) upon IR irradiation and the mixing ratio of *rim*-$HC_{20}H_{10}$ was estimated to be 1.3 ppm; three most intense lines of *rim*-$HC_{20}H_{10}$ and their predicted IR intensities were used for the estimation. The decreased amount of parent and the amount of reaction product agree with each other within errors in mixing ratio estimation; in other words, the quantum yield of the hydrogenation reaction, H + $C_{20}H_{10}$ → *rim*-$HC_{20}H_{10}$ seems to be high. The mixing ratio of HCl produced upon IR irradiation was estimated to be ~50 ppm. If we assume that the mixing ratio of H atoms thus produced was comparable to that of HCl, it was much larger than the mixing ratio of the hydrogenated product (i.e., the amount of H atoms reacted), indicating that most H-atoms were consumed in the H_2 recombination reactions.

In one experiment with electron-bombarded $C_{20}H_{10}/p$-H_2, the mixing ratio of *rim*-$HC_{20}H_{10}$ after deposition was estimated to be 1.7 ppm. After maintenance of the matrix in darkness for 30 h, the mixing ratio of *rim*-$HC_{20}H_{10}$ increased to 2.0 ppm (an increase of 0.3 ppm), corresponding to relative increase ~20 %. In contrast, the mixing ratio of $C_{20}H_{10}$ decreased from 3.0 to 2.2 ppm (a decrease of 0.8 ppm). This decrease (0.8 ppm) is much greater than the increase of *rim*-$HC_{20}H_{10}$ (0.3 ppm), even though the errors in the estimation of mixing ratios based on theoretically predicted IR intensities might be as large as a factor of two. One possibility for the decrease of $C_{20}H_{10}$ might be due to side reactions leading to other products such as a carrier of lines in group B. However, it is difficult to

elucidate the exact mechanism and to estimate the contribution from H + $C_{20}H_{10}$ → *rim*-$HC_{20}H_{10}$ reaction in darkness because, in our experiments, we observed only the time-integrated variation of species.

For protonated species *hub*-$H^+C_{20}H_{10}$ and *rim*-$H^+C_{20}H_{10}$, the mixing ratios after deposition were 0.14 and 0.10 ppm, respectively;[28] after 30 h in darkness, the mixing ratios decreased to 0.03 ppm (a decrease of 0.11 ppm) and 0.02 ppm (a decrease of 0.08 ppm), respectively. The absence of *hub*-$HC_{20}H_{10}$ in electron bombardment experiments indicated that this isomer was not produced by the neutralization of *hub*-$H^+C_{20}H_{10}$. The increase of *rim*-$HC_{20}H_{10}$ (0.3 ppm) after 30 h in darkness is significantly more than the decrease of *rim*-$H^+C_{20}H_{10}$ (0.08 ppm), but is comparable to the sum of decreases of *hub*- and *rim*-$H^+C_{20}H_{10}$ (0.19 ppm), considering the possible errors in the estimates. These results indicate two possibilities: (i) Neutralization of *hub*-$H^+C_{20}H_{10}$ involves isomerization from *hub*- to *rim*-isomer, though neutralization-induced isomerization has not been identified for other H^+PAH in solid *p*-H_2. (ii) Neutralization reaction proceeds via dissociation followed by recombination; i.e., *hub*-$H^+C_{20}H_{10}$ + e^- → H + $C_{20}H_{10}$ → *rim*-$HC_{20}H_{10}$. This mechanism is consistent with the preferential formation of *rim*-$HC_{20}H_{10}$ from H + $C_{20}H_{10}$ in the Cl_2/$C_{20}H_{10}$/*p*-H_2 experiment and the absence of *hub*-$HC_{20}H_{10}$ after deposition in the electron bombardment experiment.

So far, we are unable to provide a definitive assignment for lines in group B. These lines in group B were observed when a Cl_2/$C_{20}H_{10}$/*p*-H_2 matrix was irradiated with UV light (365 nm) followed by IR light; in contrast, visible (405 nm) and IR irradiation led to the formation of lines only in group A.

Furthermore, the lines in group B were observed only after IR irradiation. These results indicate that these lines in group B should originate from the hydrogenation reaction of fragments of $C_{20}H_{10}$ produced via photolysis at 365 nm.[28] From Table III, lines in group B show some similarity to those in group A.

VI. CONCLUSION

Electron bombardment during the deposition at 3.2 K of a mixture of $C_{20}H_{10}$ and excess *p*-H_2 produced hydrogenated species *rim*-$HC_{20}H_{10}$, in addition to protonated species *hub*-$H^+C_{20}H_{10}$ and *rim*-$H^+C_{20}H_{10}$. IR lines in two groups (A and B) were identified according to the fractional increase of intensity when the matrix was maintained in darkness. The lines in group A are assigned to *rim*-$HC_{20}H_{10}$ based on the expected chemistry and comparison with the scaled harmonic vibrational wavenumbers and IR intensities predicted with the B3PW91/6-311++G(2d,2p) method. In experiments with a $Cl_2/C_{20}H_{10}/p$-H_2 matrix, irradiated with light at 405 nm followed by IR light to generate H-atoms for reaction with $C_{20}H_{10}$, only *rim*-$HC_{20}H_{10}$ was observed. Although the bands near 3.3 and 3.4 μm of *rim*-$HC_{20}H_{10}$ agree with the UIR bands, other bands do not match satisfactorily with the UIR bands.

The quantum-chemical computations predicted that barrier heights (10.7 and 10.9 kJ mol^{-1}, respectively) for the formation of *hub*-$HC_{20}H_{10}$ and *rim*-$HC_{20}H_{10}$ are similar, but only the formation of *rim*-$HC_{20}H_{10}$ in the reaction H + $C_{20}H_{10}$ was observed. This preference in the tunneling

hydrogenation reaction might originate from the greater density of states for the formation of *rim*-$HC_{20}H_{10}$, whose energy is lower than *hub*-$HC_{20}H_{10}$ by ~17 kJ mol^{-1}.

The mechanisms for the formation of *rim*-$HC_{20}H_{10}$ in electron-bombarded $C_{20}H_{10}$/*p*-H_2 matrices were discussed according to its estimated mixing ratio at each stage of the experiments. Stoichiometric considerations on *rim*-$HC_{20}H_{10}$, *hub*-$H^+C_{20}H_{10}$, and *rim*-$H^+C_{20}H_{10}$ identified in the matrix and especially the absence of *hub*-$HC_{20}H_{10}$ indicate that, upon neutralization of *hub*-$H^+C_{20}H_{10}$, isomerization of *hub*-$HC_{20}H_{10}$ to *rim*-$HC_{20}H_{10}$ and/or a dissociative recombination reaction followed by a hydrogenation reaction to form *rim*-$HC_{20}H_{10}$ might occur.

SUPPLEMENTAL MATERIAL

Predicted absorption spectra of *hub*-$HC_{20}H_{10}$, *rim*-$HC_{20}H_{10}$, *spoke*-$HC_{20}H_{10}$, and *concave-spoke*-$HC_{20}H_{10}$ in the UV-Vis region (Fig. S1). Infrared spectra of the electron-bombarded $C_{20}H_{10}$/*p*-H_2 matrix in region 3150–2750 cm^{-1} (Fig. S2). Comparison of infrared spectra in the 1510−500 cm^{-1} region measured in a hydrogen-addition experiment and in an electron-bombardment experiment. (Fig. S3). Comparison of lines in groups A and B produced upon electron bombardment with simulated spectra in regions 1500–500 cm^{-1} (Fig. S4) and 3150–2750 cm^{-1} (Fig. S5). Comparison of infrared stick spectra of *rim*-$HC_{24}H_{12}$ and *rim*-$HC_{20}H_{10}$ (Fig. S6). Comparison of experimental vibrational wavenumbers and relative IR intensities of lines in group A with corresponding predicted

values for *rim*-$HC_{20}H_{10}$ (Table SI). Calculated vibrational wavenumbers and IR intensities of *hub*-$HC_{20}H_{10}$, *spoke*-$HC_{20}H_{10}$, and *concave-spoke*-$HC_{20}H_{10}$ (Table SII).

ACKNOWLEDGEMENTS

This work was supported by Ministry of Science and Technology, Taiwan (grant No. MOST106-2745-M009-001-ASP and MOST107-3017-F009-003) and the Center for Emergent Functional Matter Science of National Chiao Tung University from The Featured Areas Research Center Program within the framework of the Higher Education Sprout Project by the Ministry of Education (MOE) in Taiwan. Japan Society for the Promotion of Science (JSPS KAKENHI grant No. JP18K03717) partially supported this work. The National Center for High-Performance Computation of Taiwan and the Information Initiative Center of Hokkaido University provided computer time.

TABLE I. Relative energies of mono-hydrogenated corannulene isomers and transition states (TS) for isomerization computed with the B3PW91/6-311G++(2d,2p) method.[a]

Isomer[b]	Relative energy / kJ mol^{-1}	Barrier for formation[c] / kJ mol^{-1}
rim	0.0	10.9,[d] 16.0[e]
hub	17.2	10.7
spoke	64.4	22.4
concave-spoke	127.3	45.8
TS1 (*spoke–rim*)	170.6	
TS2 (*hub–spoke*)	198.1	
TS3 (*rim–concave-spoke*)	188.4	

[a]Zero-point vibrational energies are corrected using unscaled harmonic vibrational wavenumbers.

[b]See Fig. 1 for hydrogenation sites.

[c]Energy of the transition state relative to that of H + $C_{20}H_{10}$.

[d]Hydrogen atom approaching from the convex side.

[e]Hydrogen atom approaching from the concave side.

TABLE II. Representative vibrational wavenumbers (cm^{-1}) and relative IR intensities of *rim*-, *hub*-, and *spoke*-$HC_{20}H_{10}$ predicted with the B3PW91/6-311++G(2d,2p) method.[a,b]

rim-$HC_{20}H_{10}$		*hub*-$HC_{20}H_{10}$		*spoke*-$HC_{20}H_{10}$	
Mode	cm^{-1} (Int.)[c]	Mode	cm^{-1} (Int.)[c]	Mode	cm^{-1} (Int.)[c]
CH stretch					
ν_2	3052.5 (68)	ν_2	3054.1 (44)	ν_2	3053.2 (72)
ν_3	3052.1 (19)	ν_3	3053.4 (48)	ν_3	3052.3 (17)
ν_4	3051.0 (26)	ν_4	3052.9 (16)	ν_4	3046.2 (76)
ν_{10}	2916.6 (24)	ν_{11}	2785.3 (14)	ν_8	3035.6 (11)
ν_{11}	2828.3 (29)			ν_{11}	2717.0 (24)
CC stretch, CH_2 Scissor, CH in-plane bend					
ν_{18}	1457.1 (12)	ν_{38}	1143.7 (11)	ν_{19}	1472.1 (10)
ν_{19}	1449.7 (10)			ν_{20}	1440.5 (10)
ν_{23}	1413.6 (8)			ν_{29}	1301.4 (19)
ν_{24}	1407.2 (8)			ν_{30}	1274.6 (19)
ν_{30}	1297.4 (11)			ν_{40}	1125.5 (13)
CH out-of-plane bend, Ring deform					
ν_{53}	835.2 (22)	ν_{53}	829.5 (100)	ν_{45}	976.6 (19)
ν_{54}	827.0 (100)	ν_{55}	806.3 (9)	ν_{52}	847.2 (87)
ν_{57}	786.1 (16)	ν_{57}	788.8 (13)	ν_{54}	823.3 (100)
ν_{63}	651.0 (23)	ν_{58}	775.4 (11)	ν_{56}	801.5 (31)
ν_{64}	638.4 (14)	ν_{59}	744.8 (9)	ν_{57}	798.4 (9)
ν_{66}	624.7 (10)	ν_{63}	668.0 (23)	ν_{58}	786.7 (10)
ν_{71}	537.2 (22)	ν_{64}	642.3 (14)	ν_{63}	660.6 (30)
		ν_{72}	529.0 (23)	ν_{65}	635.1 (44)
				ν_{71}	549.7 (35)

[a]Vibrational modes with relative intensities ~10 % and higher are listed. Tables SI (*rim*) and SII (*hub* and *spoke*) present lists of all vibrational modes.
[b]Harmonic vibrational wavenumbers are scaled with factors 0.958 and 0.978 for regions above and below 2500 cm^{-1}, respectively.
[c]The predicted IR intensities in parentheses are normalized to the listed intensity of the most intense line in each species: *rim* (ν_{54}), 72.3 km mol^{-1}; *hub* (ν_{53}), 93.6 km mol^{-1}; *spoke* (ν_{54}), 52.7 km mol^{-1}.

TABLE III. Comparison of experimental vibrational wavenumbers (cm^{-1}) and relative IR intensities of *rim*-$HC_{20}H_{10}$ (group A) with corresponding values predicted with the B3PW91/6-311++G(2d,2p) method. Lines of group B are also listed for comparison.

Mode[a]	Calculated[b]	Group A		Group B
		$C_{20}H_{10}$/*p*-H_2 (e^- bombardment)	Cl_2/$C_{20}H_{10}$/*p*-H_2 (Vis/IR)	$C_{20}H_{10}$/*p*-H_2 (e^- bombardment)
ν_2	3052.5 (68)[c]	3051.2?[d] (47)[e]	3051.2?[d] (51)[e]	3053.9[d] (45)[e]
ν_3	3052.1 (19)	3051.2?[d] (47)	3051.2?[d] (51)	
ν_4	3051.0 (26)	3048.1 (15)	3048.1 (15)	3039.9[d] (45)
ν_7	3035.6 (4)	3030.1 (5)	3030.1 (5)	
ν_{10}	2916.6 (24)	2908.2 (10)	–[f]	
ν_{11}	2828.3 (29)	2792.3 (11)	2792.3 (10)	2820.8 (8)
ν_{29}	1311.6 (7)	1311.3[g] (7)	1311.3 (6)	1307.8 (1)
ν_{30}	1297.4 (11)	1299.4 (5)	1299.4 (8)	
ν_{31}	1280.9 (6)	1277.8 (2)	1277.8 (2)	
ν_{32}	1225.3 (4)	1223.3 (3)	1223.3 (3)	
ν_{36}	1166.2 (3)	1155.9 (3)	1155.9 (2)	1133.1 (2)
ν_{40}	1128.4 (9)	1128.4 (7)	1128.4 (8)	
ν_{41}	1125.1 (8)	1124.7 (7)	1124.7 (7)	
ν_{47}	947.5 (9)	947.5 (9)	947.5 (9)	953.4 (5)
ν_{53}	835.2 (22)	–[h]	–[h]	830.9 (4)
ν_{54}	827.0 (100)	827.1 (100)	827.1 (100)	822.7 (100)
ν_{55}	811.7 (8)	807.8 (9)	807.8 (8)	803.2 (9)
ν_{56}	805.0 (3)	795.4 (3)	795.4 (3)	
ν_{57}	786.1 (16)	788.9 (19)	788.9 (17)	777.6 (13)
ν_{58}	763.8 (6)	768.3 (11)	768.3 (10)	761.7 (11)
ν_{59}	748.9 (3)	734.1 (3)	734.1 (3)	
ν_{63}	651.0 (23)	652.4 (24)	652.4 (24)	656.4 (14)
ν_{64}	638.4 (14)	638.6 (14)	638.6 (14)	
ν_{65}	630.0 (3)	632.3 (4)	632.3 (4)	642.3 (3)
ν_{66}	624.7 (10)	627.5 (11)	627.5 (11)	631.8 (2)
ν_{71}	537.2 (22)	536.4 (10)	536.4 (7)	595.1 (3)
ν_{72}	532.9 (4)	534.0 (6)	534.4 (5)	
ν_{73}	526.0 (7)	528.5 (8)	528.5 (7)	

[a]Table S1 presents a list of all vibrational modes.
[b]Harmonic vibrational wavenumbers are scaled with factors 0.958 and 0.978 for regions above and below 2500 cm^{-1}, respectively.
[c]The predicted IR intensities in parentheses are normalized to the intensity of the most intense line (ν_{54}) with IR intensity 72.3 km mol^{-1}.

[d]Assignments are tentative because of spectral congestion in the CH stretching region.
[e]Integrated IR intensities as a percentage of the most intense line at 826.4 cm^{-1} are listed in parentheses.
[f]Unobserved because of severe interference from $(HCl)_n$.
[g]The increase of this line in darkness was unidentified because of severe interference from $H^+C_{20}H_{10}$ and $C_{20}H_{10}$.
[h]Unobserved because of the interference with the most intense line of $C_{20}H_{10}$ near 837 cm^{-1}.

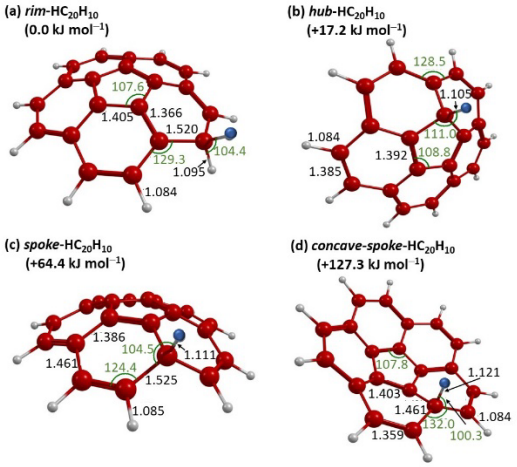

FIG. 1. Geometries of (a) *rim*-$HC_{20}H_{10}$, (b) *hub*-$HC_{20}H_{10}$, (c) *spoke*-$HC_{20}H_{10}$, and (d) *concave-spoke*-$HC_{20}H_{10}$ optimized with the B3PW91/6-311++G(2d,2p) method. The ZPVE-corrected relative energies (in kJ mol^{-1}) are listed in parentheses. Bond lengths and angles are in Å and degree, respectively.

(Single column)

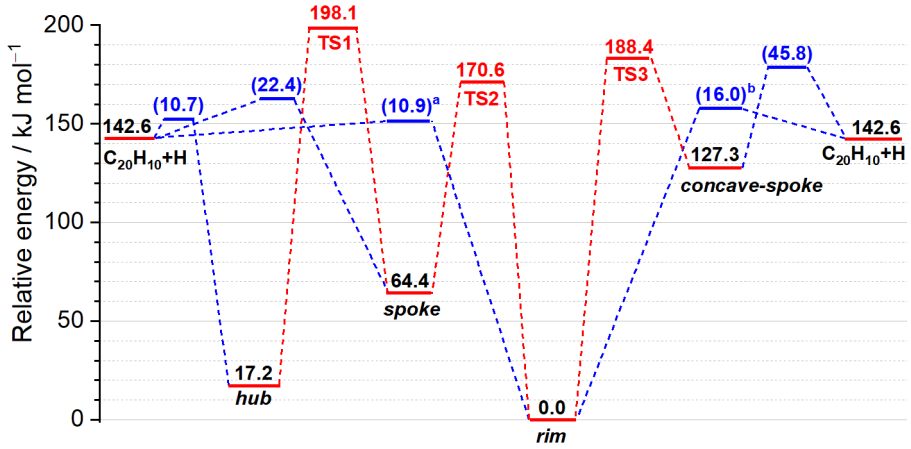

FIG. 2. Calculated relative energies of hydrogenated corannulene isomers (*rim*-, *hub*-, *spoke*-, and *concave-spoke*-$HC_{20}H_{10}$) and transition states connecting them. Calculations were performed with the B3PW91/6-311++G(2d,2p) method; zero-point vibrational energies were corrected with unscaled harmonic vibrational energies. Blue traces indicate hydrogen-addition reaction and red traces indicate isomerization. The values in parentheses are barrier heights relative to $C_{20}H_{10}$ + H. The formation of the *rim*-isomer can occur either via hydrogen atom approaching from the convex side (marked as *a*) and from the concave side (marked as *b*).

(double column)

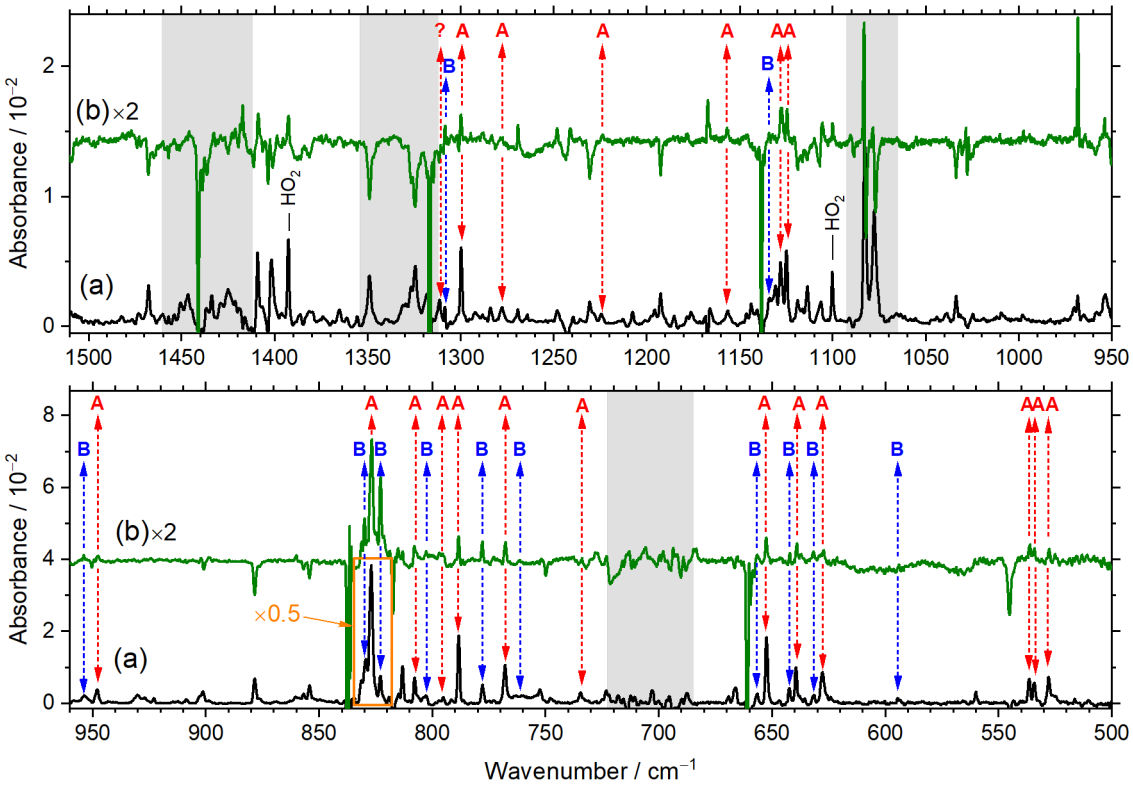

FIG. 3. Infrared spectra of electron-bombardment experiments on $C_{20}H_{10}$/*p*-H_2 in region 1510–500 cm^{-1}. (a) IR spectrum of the electron-bombarded matrix with lines of $C_{20}H_{10}$ subtracted using an IR spectrum of $C_{20}H_{10}$/*p*-H_2 matrix deposited without electron bombardment; (b) difference spectrum of the electron-bombarded matrix after maintenance in darkness at 3.2 K for 30 h; lines pointing upward indicate production and those pointing downward indicate destruction. The lines in groups A and B are indicated with red and blue arrows, respectively. Tentative assignments are indicated with "?". The lines near 1100 and 1392 cm^{-1} due to HO_2, which originated from the hydrogenation of O_2 impurity, are also indicated. Negative lines in trace (b) are due to $C_{20}H_{10}$ or $H^+C_{20}H_{10}$ for which spectral assignments were presented in our previous work.[28] The regions suffering from extensive interference are indicated with grey rectangles.

(Double column)

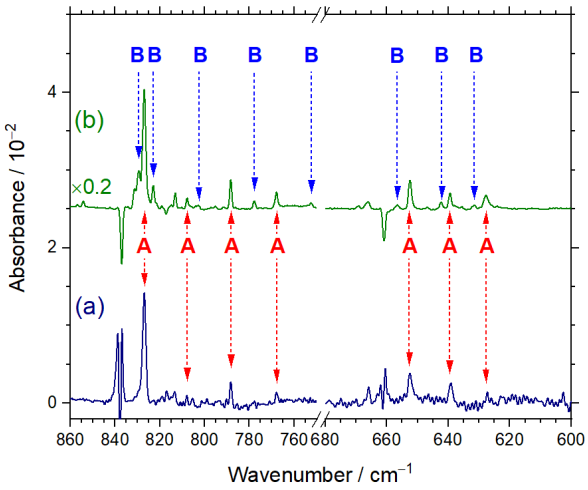

FIG. 4. Comparison of IR spectra in regions 860–750 and 680–600 cm^{-1} measured for a hydrogen-addition experiment and an electron-bombardment experiment. (a) The IR spectrum of $Cl_2/C_{20}H_{10}/p\text{-}H_2$ matrix after visible (405 nm) and IR irradiation. (b) The spectrum of the electron-bombarded $C_{20}H_{10}/p\text{-}H_2$ matrix after maintenance in darkness at 3.2 K for 30 h. From both traces, the lines of $C_{20}H_{10}$ were stripped. The lines in groups A and B are indicated with red and blue arrows, respectively.

(Single column)

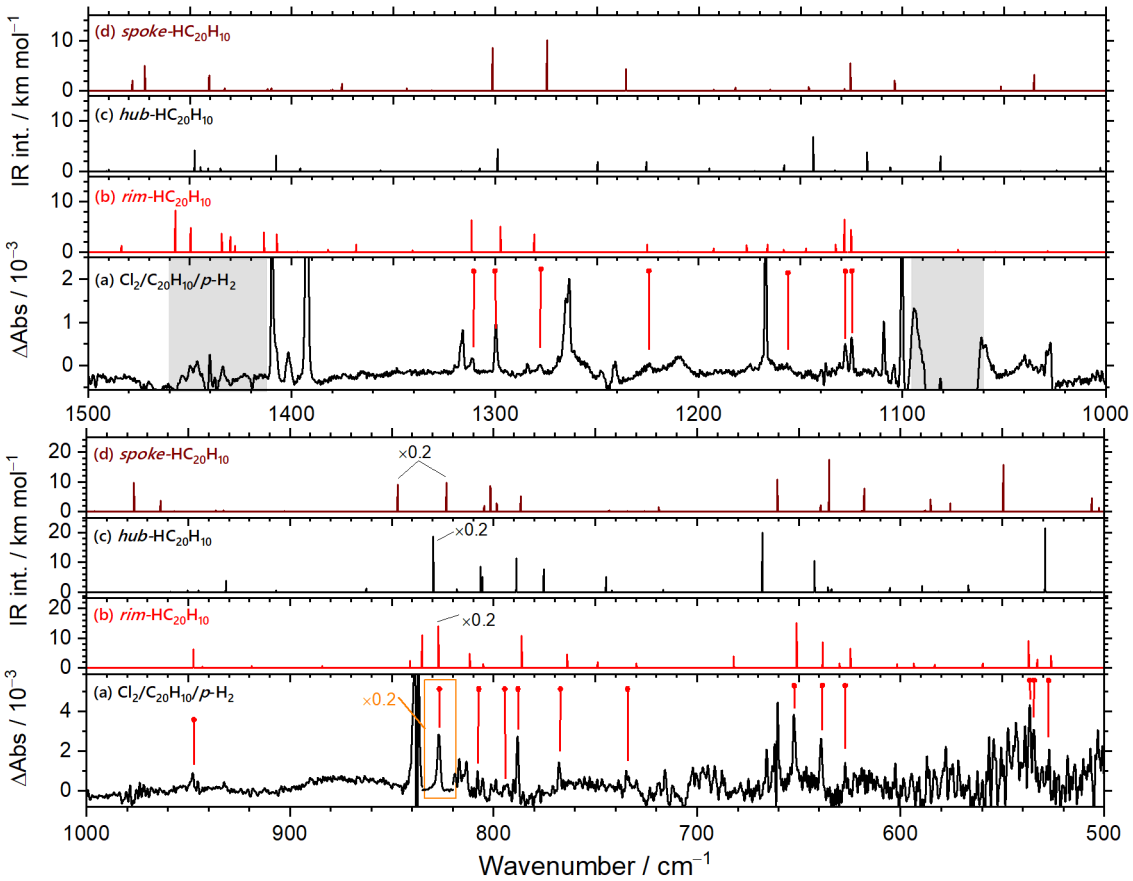

FIG. 5. Comparison of an experimental IR spectrum with simulated spectra in region 1500–500 cm^{-1}. (a) The IR spectrum of a $Cl_2/C_{20}H_{10}/p$-H_2 matrix after visible (405 nm) and IR irradiation; the lines of $C_{20}H_{10}$ were stripped and lines in group A are indicated by red dots. Infrared stick spectra of (b) *rim*-$HC_{20}H_{10}$, (c) *hub*-$HC_{20}H_{10}$, and (d) *spoke*-$HC_{20}H_{10}$ simulated according to scaled harmonic vibrational wavenumbers and IR intensities predicted with the B3PW91/6-311++G(2d,2p) method; see text. In (a), the regions suffering from extensive interference are indicated with grey rectangles.

(Double column)

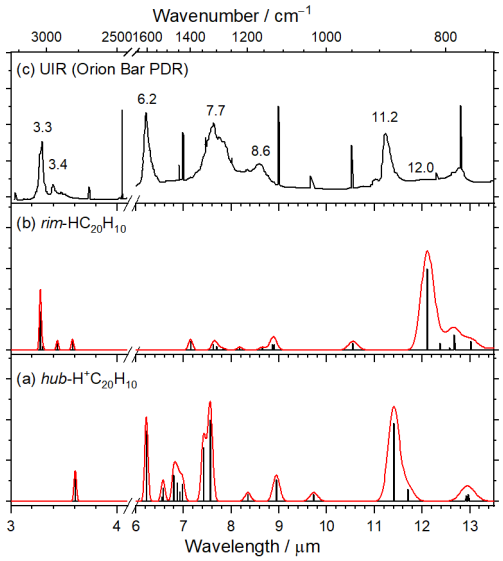

FIG. 6. Comparison of UIR bands with experimental IR spectra of hydrogenated and protonated corannulene in solid *p*-H_2. Experimental spectra of (a) *hub*-$H^+C_{20}H_{10}$[28] and (b) *rim*-$HC_{20}H_{10}$; (c) the UIR emission spectrum from Orion Bar PDR (Ref. 39). Experimental spectra are presented with sticks of which the heights represent integrated intensities. Solid red lines represent spectra convoluted with Gaussian profiles of full-width at half-maximum 30 cm^{-1}.

(Single column)

REFERENCES

[1] A. G. G. M. Tielens, Rev. Mod. Phys. **85**, 1021 (2013).

[2] A. G. G. M. Tielens, in *PAHs and the Universe*, edited by C. Joblin and A. G. G. M. Tielens (EAD Sciences, Les Ulis, 2011), p. 3.

[3] E. Peeters, in *PAHs and the Universe*, edited by C. Joblin and A. G. G. M. Tielens (EAD Sciences, Les Ulis, 2011), p. 13.

[4] A. Pathak and P. J. Sarre, Mon. Not. R. Astron. Soc. Lett. **391**, L10 (2008).

[5] M. P. Bernstein, S. A. Sandford, and L. J. Allamandola, Astrophys. J. Lett. **472**, L127 (1996).

[6] L. Boschman, S. Cazaux, M. Spaans, R. Hoekstra, and T. Schlathölter, Astron. Astrophys. **579**, A72 (2015).

[7] V. Le Page, T. P. Snow, and V. M. Bierbaum, Astrophys. J. **704**, 274 (2009).

[8] E. Rauls and L. Hornekær. Astrophys. J. **679**, 531 (2008).

[9] K. Bekki, Mon. Not. R. Astron. Soc. **444**, 1615 (2014).

[10] L. Boschman, G. Reitsma, S. Cazaux, T. Schlathölter, R. Hoekstra, M. Spaans, and O. González-Magaña, Astrophys. J. Lett. **761**, L33 (2012).

[11] J. H. Black and E. F. van Dishoeck, Astrophys. J. **322**, 412 (1987).

[12] J. M. Shull and S. Beckwith, Annu. Rev. Astron. Astrophys. **20**, 163 (1982).

[13] B.T. Draine and F. Bertoldi. Astrophys. J. **468**, 269 (1996).

[14] R. J. Gould, T. Gold, and E. E. Salpeter, Astrophys. J., **138**, 408 (1963).

[15] N. Katz, I. Furman, O. Biham, V. Pirronello, and G. Vidali, Astrophys. J. **522**, 305 (1999).

[16] R. J. Gould and E. E. Salpeter, Astrophys. J. **138**, 393 (1963).

[17] G. Vidali, Chem. Rev. **113**, 8762 (2013).

[18] V. Wakelam, E. Bron, S. Cazaux, F. Dulieu, C. Gry, P. Guillard, E. Habart, L. Hornekær, S. Morisset, G. Nyman, V. Pirronello, S. D. Price, V. Valdivia, G. Vidali, and N. Watanabe, Mol. Astrophys. **9**, 1 (2017).

[19] E. Habart, F. Boulanger, L. Verstraete, C. M. Walmsley, and G. Pineau des Forêts, Astron. Astrophys. **414**, 531 (2004).

[20] M. Bahou, Y.-J. Wu, and Y.-P. Lee, J. Chem. Phys. **136**, 154304 (2012).

[21] M. Bahou, Y.-J. Wu, and Y.-P. Lee, Phys. Chem. Chem. Phys. **15**, 1907 (2013).

[22] M. Bahou, Y.-J. Wu, and Y.-P. Lee, J. Chem. Phys. Lett. **4**, 1989 (2013).

[23] M. Bahou, Y.-J. Wu, and Y.-P. Lee, Angew. Chem., Int. Ed. **53**, 1021 (2014).

[24] M. Tsuge, M. Bahou, Y.-J. Wu, L. Allamandola, and Y.-P. Lee, Astrophys. J. **825**, 96 (2016).

[25] M. Bahou, P. Das, Y.-F. Lee, Y.-J. Wu, and Y.-P. Lee, Phys. Chem. Chem. Phys. **16**, 2200 (2014).

[26] M. Tsuge, M. Bahou, Y.-J. Wu, L. Allamandola, and Y.-P. Lee, Phys. Chem. Chem. Phys. **18**, 28864 (2016).

[27] G. Rouillé, C. Jäger, M. Steglich, F. Huisken, T. Henning, G. Theumer, I. Bauer, and H.-J. Knölker, ChemPhysChem **9**, 2085 (2008).

[28] P. Sundararajan, M. Tsuge, M. Baba, and Y.-P. Lee, ACS Earth Space Chem. **2,** 1001 (2018).

[29] H. Álvaro Galué and G. Díaz Leines, Phys. Rev. Lett. **119**, 171102 (2017).

[30] H. Álvaro Galué, C. A. Rice, J. D. Steill, and J. Oomens, J. Chem. Phys. **134**, 054310 (2011).

[31] M. Tsuge, C.-Y. Tseng, and Y.-P. Lee, Phys. Chem. Chem. Phys., **20**, 5344 (2018).

[32] Y.-P. Lee, Y.-J. Wu, R. M. Lees, L.-H. Xu, and J. T. Hougen, Science **311**, 365 (2006).

[33] M.-C. Chan, M. Okumura, and T. Oka, J. Phys. Chem. A **104**, 3775 (2000).
[34] B. Golec, P. Das, M. Bahou, and Y.-P. Lee, J. Phys. Chem. A **117**, 13680 (2013).
[35] P. L. Raston and D. T. Anderson, Phys. Chem. Chem. Phys. **8**, 3124 (2006).
[36] M. Ruzi and D. T. Anderson, J. Chem. Phys. **137**, 194313 (2012).
[37] C. Joblin, A. G. G. M. Tielens, L. J. Allamandola, A. Léger, L. d'Hendecourt, T. R. Geballe, and P. Boissel, Planet. Space Sci. **43,** 1189 (1995).
[38] L. J. Allamandola, D. M. Hudgins, and S. A. Sandford, Astrophys. J. Lett. **511**, L115 (1999).
[39] E. Peeters, A. L. Mattioda, D. M. Hudgins, S. Hony, and A. G. G. M. Tielens, ASP Conf. Ser. **309**, 141 (2004).